Charge order and metal-insulator transition in chiral molecular conductors (DM-EDT-TTF) 2 X, (X=ClO 4 , ReO 4)

M. Sawińska, A. Frąckowiak, I. Olejniczak, T. Runka, S. Priya, M. Dressel, F. Pop, N. Avarvari

Charge order and metal-insulator transition in chiral molecular conductors (DM-EDT-TTF)$_2$X, (X=ClO_4, ReO_4)

M. Sawińska,[1] A. Frąckowiak,[1] I. Olejniczak,[1,*] T. Runka,[2] S. Priya,[3] M. Dressel,[3] F. Pop,[4] and N. Avarvari[4]

[1] *Institute of Molecular Physics, Polish Academy of Sciences, Smoluchowskiego 17, 60-179 Poznań, Poland*
[2] *Faculty of Materials Engineering and Technical Physics, Poznan University of Technology, Piotrowo 3, 60-965 Poznań, Poland*
[3] *1. Physikalisches Institut, Universität Stuttgart, 70569 Stuttgart, Germany*
[4] *Laboratoire Moltech Anjou, UMR 6200 CNRS, Universite d'Angers, UFR Sciences, Bât. K, 2 Bd. Lavoisier, 49045 Angers, France*

(Dated: May 17, 2025)

Optical measurements reveal the charge-ordered nature of the insulating state in the chiral molecular conductors [(S,S/R,R)-DM-EDT-TTF]$_2ClO_4$ (DM-Cl) and [(S,S/R,R)-DM-EDT-TTF]$_2ReO_4$ (DM-Re). These enantiopure materials exhibit metallic conductivity at room temperature and a metal-insulator transition upon cooling below T_{MI} = 40 and 120 K, respectively. Optical conductivity spectra display a polarization-independent in-plane response, attributed to the hexagonal structure of the conducting DM-EDT-TTF layer, featuring broadband electronic excitations, molecular vibrational modes, and a Drude component in the metallic phase. The gap opening at 150 and 250 cm^{-1} for DM-Cl and DM-Re, respectively, signals the transition from a metallic to an insulating state upon cooling. Drude-Lorentz-Fano analysis of the optical spectra yields Hubbard parameters, the intersite Coulomb repulsion V and the bandwidth W, supporting the presence of charge order in the insulating phase. Raman spectra of DM-Cl and DM-Re, focusing on charge-sensitive molecular vibrations, further confirm a charge-ordered insulating state with a charge disproportionation of $0.10e$ and $0.13e$, respectively. Strong DM-EDT-TTF molecular modes, activated in optical spectra through coupling with the electronic background, support the presence of lattice frustration.

I. INTRODUCTION

The study of low-dimensional conducting materials continues to captivate solid state researchers due to their rich and complex electronic behavior. Among these, molecular conductors based on tetrathiafulvalene (TTF) derivatives stand out as key examples in the broader field of materials science. This interest is underscored by extensive research on molecular systems built from TMTSF (tetramethyltetraselenafulvalene), TMTTF (tetramethyltetrathiafulvalene), and BEDT-TTF (bisethylenedithio-tetrathiafulvalene) molecules. The materials exhibit a diverse array of phenomena, including unconventional superconductivity and various competing broken-symmetry states such as charge density waves (CDW), spin density waves (SDW), spin-Peierls (SP), charge ordering (CO), metal-insulator transitions (MIT), and spin liquid (SL) states. Such behavior highlights the intricate interplay between charge, spin, and lattice degrees of freedom, offering a rich platform for exploring fundamental physical principles [1–5].

In condensed matter physics, the electronic phases of low-dimensional molecular conductors can be finely tuned using external stimuli such as temperature, pressure, magnetic field, or light [4–8]. Recently, a novel approach involving the controlled incorporation of chirality into low-dimensional structures has emerged, creating multifunctional materials whose electronic and optical properties can be further adjusted through chirality [9]. This synthetic strategy has led to the development of chiral tetrathiafulvalene derivatives, including DM-EDT-TTF (dimethyl-ethylenedithio-tetrathiafulvalene) [10–12], DM-BEDT-TTF (dimethyl-bisethylenedithio-tetrathiafulvalene) [13], and a series of conducting chiral single-component metal-dithiolene complexes [14, 15]. Among these, the enantiopure [(S,S)-DM-EDT-TTF]$_2ClO_4$ and [(R,R)-DM-EDT-TTF]$_2ClO_4$ have shown evidence of electrical magnetochiral anisotropy (eMChA) [10], and, more recently, of the chiral-induced spin selectivity (CISS) effect [16]. Despite significant synthetic advances and a decade of intensive research, the connection between physical properties and structural characteristics in chiral molecular conductors remains insufficiently understood. Some of the materials exhibit metallic-like conductivity at higher temperatures, but as the temperature decreases, they transit into insulating phases or undergo charge localization [10–13]. Various factors may contribute to the metal-insulator phase transition in low-dimensional molecular solids, and electronic correlations can localize electrons into a Mott insulating state through strong on-site Coulomb repulsion (U) or into a charge-ordered state due to significant inter-site Coulomb repulsion (V). To date, optical studies have confirmed a Mott insulating state accompanied by charge fluctuations in (*rac*-DM-EDT-TTF)$_2PF_6$ [17].

In the present study, we focus on the chiral salts [(S,S)-DM-EDT-TTF]$_2ClO_4$, [(R,R)-DM-EDT-TTF]$_2ClO_4$, [(S,S)-DM-EDT-TTF]$_2ReO_4$, and [(R,R)-DM-EDT-TTF]$_2ReO_4$, referred to as DM-Cl and DM-Re depending on the anion. These quarter-filled materials possess metallic conductivity at room temperature

* olejniczak@ifmpan.poznan.pl

and metal-insulator phase transition (MIT) at T_{MI} = 40 K and 120 K, respectively [10, 16]. Both salts crystallize in hexagonal space groups $P6_222$ and $P6_422$ for the (S,S) and (R,R) enantiomers, respectively. At room temperature, the bond lengths align with a mixed valence state of $+0.5e$ per donor molecule, consistent with the 2:1 stoichiometry. Band-structure and Fermi surface calculations based on the room-temperature crystal structure predicted that the low-temperature insulating behavior of DM-Cl may be associated with charge- or spin-density-wave (CDW/SDW) instabilities [10]. More recent work on DM-Re, involving low-temperature band-structure calculations and magnetic susceptibility measurements, supports a charge-order (CO) scenario [16]. Interestingly, similar low-temperature calculations for DM-Cl do not predict CO, and the origin of this difference between the two compounds remains to be clarified [16].

Here, we provide detailed insights into low-frequency electronic excitations and charge-sensitive molecular vibrations through comprehensive infrared optical and Raman spectroscopy investigations. Our findings reveal vibrational signatures of charge ordering, quantify the dominant electronic correlations, and highlight the role of lattice frustration in electron-molecular vibration (*emv*) interactions.

II. EXPERIMENTS AND METHODS

High quality single crystals of the enantiopure salts [(S,S)-DM-EDT-TTF]$_2ClO_4$, [(R,R)-DM-EDT-TTF]$_2ClO_4$, [(S,S)-DM-EDT-TTF]$_2ReO_4$, and [(R,R)-DM-EDT-TTF]$_2ReO_4$ have been prepared by electrocrystallization using the method described previously [10, 16]. Since we do not utilize circular polarized radiation and magnetism does not play a role in our optical experiments, we do not observe chirality-dependent effects. Thus, we consider all measured values to be chirality-independent and use the simplified compound names DM-Cl and DM-Re, regardless of the sample's chirality. Single-crystalline samples for optical measurements were prepared as shiny platelets with typical dimensions of 1 × 0.5 × 0.2 mm^3, with their best-developed *ab* crystal face oriented parallel to the DM-EDT-TTF conducting layers. Variable-temperature close-to-normal incidence reflectivity measurements were conducted down to 10 K over a frequency range of 100 - 15000 cm^{-1} using a Bruker Vertex 80v Fourier-transform spectrometer, equipped with a microscope, helium cryostat, and a range of detectors, including a bolometer for the far-infrared range. Freshly evaporated gold mirrors served as references. Preliminary measurements confirmed no polarization dependence within the conducting plane, consistent with the specific twisted arrangement of the hexagonal structure [10, 16]. Consequently, the "in-plane" reflectivity was finally measured without the use of a polarizer. The optical conductivity $\sigma_1(\omega)$ was derived from Kramers-Kronig analysis of the reflectance data, with appropriate low-frequency extrapolations applied for the metallic and insulating phases [18]. Raman spectra were collected from the best-developed crystal face over the frequency range of 300 - 1700 cm^{-1} using backscattering geometry. Measurements were conducted with two Raman spectrometers: a LABRAM HR800 with a 632.8 nm excitation laser and a Renishaw inVia with a 785 nm excitation laser, both equipped with microscopes and a helium cryostat. The spectral resolution achieved was better than 2 cm^{-1}. To prevent overheating of the samples, the laser power was reduced to approximately 0.2 mW. Raman intensity was converted to Raman susceptibility using the Bose-Einstein factor for accurate temperature dependent analysis.

III. MATERIALS

Figure 1(a) shows a characteristic hexagonal crystal structure of DM-Cl and DM-Re in the *ab* plane [10]. The unit cell of these layered molecular materials is composed of the conducting *ab* layers of DM-EDT-TTF donors and insulating anion layers, spanning through three conducting layers. At room temperature, the metallic phase contains six donor molecules per unit cell, with two per conducting *ab* layer [10, 16]. These molecules interact strongly, forming uniform stacks along the *a*-direction which are coupled through half as weak interstack interactions along the *b*-direction. As the temperature decreases below T_{MI}, the unit cell expands due to a symmetry reduction, leading to a doubling of the lattice parameters along both *a* and *b* (space groups $P6_2$ or $P6_4$). The low-temperature unit cell comprises twenty four donor molecules, with eight per *ab*-layer [16].

Molecular arrangement of the conducting layer below T_{MI} of both DM-Cl and DM-Re is characterized by the presence of four different donor molecules labeled A, B, C, D (Fig. 1(d)). This results in fourteen main interactions, with four the strongest almost uniform along the donor stacks (Fig. 1(d), 1(e), interactions I-IV) [16]. Weak dimerization resulting in AD and BC dimers, and possible charge disproportionation is suggested by recent band structure calculations [16]. Both DM-Cl and DM-Re undergo a metal-insulator phase transition as revealed by the temperature dependence of the dc resistivity on cooling below T_{MI} = 40 K and 120 K, respectively (Fig. 1(c)) [16]. The most prominent vibrational features of DM-EDT-TTF donor molecule are the C=C stretching modes, based on similar mode patterns of BEDT-TTF in D_{2h} molecular symmetry labeled as ν_2, ν_3 and ν_{27} (Fig. 1(b)) [11, 17]. These vibrational modes are active both in Raman and optical conductivity spectra due to the low symmetry of DM-EDT-TTF. Here the ν_2 and ν_{27} modes characterized by strong frequency dependence on charge can be used for estimation of charge localized on DM-EDT-TTF. On the other hand, the ν_3 mode is sensitive to structure modification.

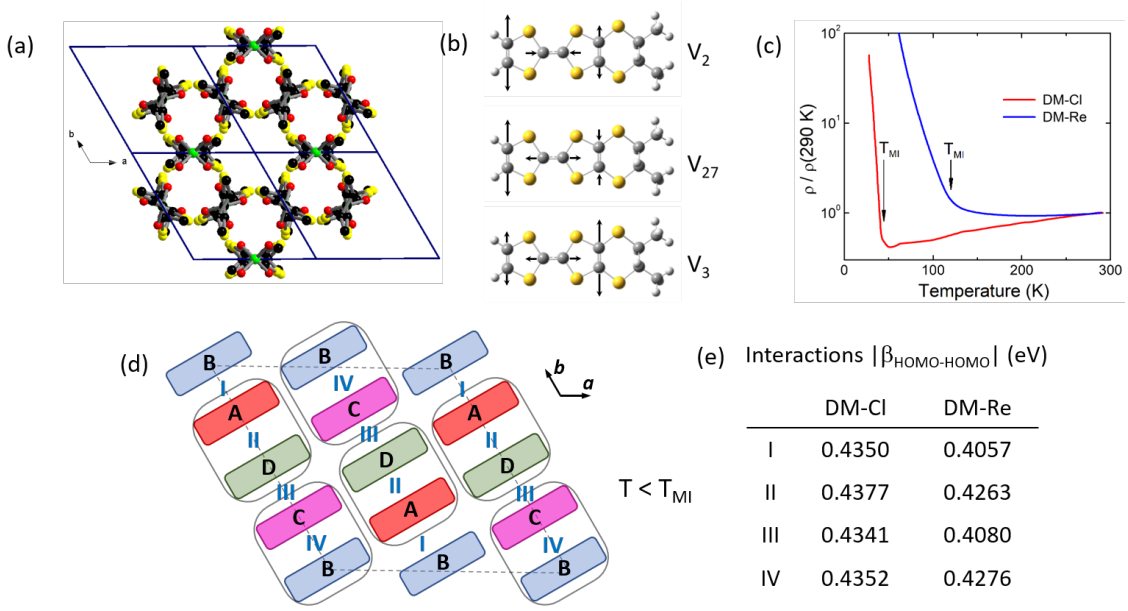

	DM-Cl	DM-Re
I	0.4350	0.4057
II	0.4377	0.4263
III	0.4341	0.4080
IV	0.4352	0.4276

Figure 1. The unit cell of the crystal structure of DM-Cl and DM-Re spans three conducting layers. (a) The packing diagram of DM-Cl in the *ab* plane shows hexagonal symmetry (H atoms are omitted for clarity) [10, 16]. (b) Calculated C=C stretching mode patterns of DM-EDT-TTF (dimethyl-ethylenedithio-tetrathiafulvalene) molecule, based on Ref. [11]. The ν_2 and ν_{27} modes are sensitive to local charge and can be used to estimate charge disproportionation; ν_3 is sensitive to structural changes. (c) Temperature dependence of the normalized dc resistivity of DM-Cl and DM-Re, indicating metal–insulator transitions at T_{MI} = 40 K and 120 K, respectively. Data for DM-Cl are from Ref. [10]; DM-Re data are unpublished (Ref. [16], courtesy of co-authors). (d) Molecular arrangement within the conducting layers in the insulating phase, showing four crystallographically distinct donor molecules (A–D) coupled via fourteen dominant intermolecular pathways [16]. The stacking is quasi-one-dimensional along the *b*-axis, with stronger in-stack I-IV interactions than those along the *a*-direction (not shown). Weak dimerization (AD and BC) and charge order are suggested, with charge-rich molecules colored red/magenta and charge-poor blue/green [16]. (e) Absolute values of the HOMO–HOMO transfer integrals $\beta_{HOMO-HOMO}$ (in eV) for in-stack donor-donor interactions (I-IV) in the 18 K structures of DM-Cl and DM-Re, based on Ref. [16].

IV. RESULTS AND DISCUSSION

Figure 2 presents the in-plane reflectance and corresponding broadband optical conductivity spectra of DM-Cl and DM-Re at 300 K (conducting state) and 11 K (insulating state). The room-temperature reflectance spectra of both materials (Fig. 2(a), 2(b)) show a response typical of low-dimensional organic metals, with a characteristic rise in reflectance to values of 0.6 - 0.8 at low frequencies. This metallic signature diminishes as the system transitions into the insulating phase. At 11 K, the reflectance becomes flat at low frequencies, consistent with the expected behavior of an insulator. Note that unpolarized spectra presented in this work include contributions of the electronic response both in the stack *b* and the interstack *a* directions within the crystal structure (Fig. 1(d)). While they cannot be easily separated, we assume that the most of the optical response is related with the stack *b* direction due to significantly stronger interactions [16].

A key feature of the 300 K optical conductivity spectra for both DM-Cl and DM-Re (Fig. 2(c), 2(d)) is a broad mid-infrared band extending from 600 to 4000

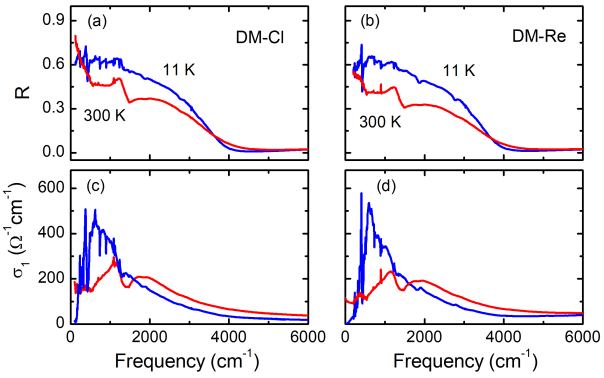

Figure 2. Metal-insulator phase transition in DM-Cl (a,c) and DM-Re (b,d) as revealed by in-plane optical reflectivity measurements at 300 K (metallic state) and 11 K (insulating state). Panels (a) and (b) show the reflectance spectra, while (c) and (d) present the corresponding optical conductivity spectra. At 300 K, the spectra exhibit features characteristic of an organic metal. Upon cooling, a gap opens in the far-infrared range, accompanied by a redistribution of spectral weight and the appearance of pronounced vibrational modes, signaling the transition to an insulating state.

cm^{-1}, with a center at ∼1500 cm^{-1} and a plasma frequency $\omega_p \sim 4000$ cm^{-1}. This band exhibits a pronounced depression at 1400 cm^{-1}, a characteristic feature commonly observed in BEDT-TTF salts [19]. The dip arises from electron-molecular vibration (*emv*) coupling, specifically involving the double C=C stretching ν_3 mode of the donor molecule interacting with the low-energy electronic background within the dimerized structure [20]. Both DM-Cl and DM-Re display finite conductivity at zero frequency, consistent with their metallic nature [21]. When the temperature decreases from 300 K to 11 K, three significant modifications are observed in the optical response: (1) a substantial redistribution of the spectral weight (SW), (2) the opening of a gap at the metal-insulator transition temperature, and (3) the appearance of strong vibrational DM-EDT-TTF modes in the frequency range below 1000 cm^{-1}.

A. Optical spectra: Metal-insulator transition

Figure 3 presents the temperature-dependent evolution of the in-plane optical conductivity for DM-Cl (panels a, b) and DM-Re (panels c, d) across their metal-insulator transitions, which occur at T_{MI} = 50 K and 100 K, respectively. Both compounds exhibit qualitatively similar behavior throughout the transition: a prominent mid-infrared excitation progressively shifts to lower frequencies as the temperature approaches T_{MI}, below which an insulating gap emerges. In the insulating phase, the conductivity spectra are characterized primarily by a band centered at ∼600 cm^{-1} and distinct vibrational modes (Fig. 3(a), 3(c)). We estimate the insulating gap, Δ_{MI}, by linearly extrapolating the low-frequency edge of the optical conductivity in the insulating phase, yielding Δ_{MI} values of approximately 150 cm^{-1} for DM-Cl and 250 cm^{-1} for DM-Re. Notably, these gap values align well with activation energies E_a = 260 and 305 cm^{-1}, respectively, as determined from transport measurements [16].

Modifications in the electrodynamic response at T_{MI} are clearly shown in the optical conductivity contour plots (Fig. 3(b), 3(d)), which include values of the spectral weight center, $<\omega> = \int_{100}^{3000}\omega\sigma_1(\omega)d\omega$ / $\int_{100}^{3000}\sigma_1(\omega)d\omega$. Starting from room temperature in the metallic state, the spectral weight center for both DM-Cl and DM-Re shifts linearly towards lower frequencies as the temperature decreases to T_{MI}; specifically, $<\omega>$ decreases from approximately 1510 cm^{-1} at 300 K to 1220 cm^{-1} at 60 K for DM-Cl, and from approximately 1590 cm^{-1} at 300 K to 1230 cm^{-1} at 100 K for DM-Re. Upon entering the insulating phase, $<\omega>$ initially shifts upward with further temperature reduction, signaling the onset of the gap opening at T_{MI}. However, this upturn is followed by a renewed downshift, with $<\omega>$ reaching approximately 1240 cm^{-1} for DM-Cl, and 1150 cm^{-1} for DM-Re) at 11 K, indicating the complete development of the insulating gap.

In correlated materials, the broadband electronic excitation observed in optical conductivity spectra reveals insights into the strength of Coulomb correlations. For a half-filled Mott insulator, the Hubbard model predicts an absorption band with the bandwidth $2W$ arising from interband transitions between two Hubbard bands, each characterized by the bandwidth W, separated in the density of states (DOS) by the on-site Coulomb repulsion U [22, 23]. On the other hand, weakly dimerized quarter-filled conductors characterized by significant intersite Coulomb repulsion V, are described within the extended Hubbard model relevant for DM-Cl and DM-Re, that yields a broadband peak centered at the frequency related with both U and V [24, 25]. In fact, recent optical studies of charge-ordered β''-type BEDT-TTF salts demonstrate that the optical response in these systems can be understood in terms of the Mott-Hubbard band centered at the effective value of $U - V$ or V, depending on the CO pattern [26, 27].

Within the Hubbard framework, we consider that the electronic response of DM-Cl and DM-Re is characterized by the coherent quasiparticle Drude contribution in the metallic phase, accompanied by a broad middle infrared peak that indicates excitations between the Hubbard bands. Considering the shape and temperature dependence, we assume that its frequency at maximum ω^{max} corresponds to the Coulomb repulsion value V [26, 28]. The bandwidth W of this Mott-Hubbard band is estimated as half-width at half-height from the low-frequency side [25, 28]. The correlation strength is calculated based on the ratio V/W. To extract these values we modeled the spectra with a Drude-Lorentz-Fano approach, including a standard Drude term to represent the coherent quasiparticle response, two Lorentzian functions for a mid-infrared peak, and a set of Fano functions, adjusted by temperature, to capture the vibrational features that strongly interact with the electronic background in our systems.

Figure 4 shows the fit quality for DM-Cl at 300 K (panel a) and 11 K (panel b), along with individual contributions from Drude, Lorentz, and Fano components at 300 K (panel c) and 11 K (panel d) (data for DM-Re are shown in Fig. S1 in Supplementary Information [29]). Notably, the Drude component is weak, consistent with a low DC conductivity value of σ_{dc} = 10 - 30 Ω^{-1}cm^{-1} at room temperature [16, 21]. The Fano term accounts for the vibrational modes, which will be discussed in detail in a separate section. The Lorentz contribution, representing the Mott-Hubbard band through two combined Lorentzians L1 and L2 (Fig. S2 in Supplementary Information [29]), with Hubbard parameters V and W indicated, is shown in Figs. 4(c) and 4(d).

The estimated values at 300 and 11 K indicate that, in all cases, the intersite Coulomb repulsion V exceeds the bandwidth W (Tab. I), suggesting significant effective correlations even in the metallic phase at room temperature. For DM-Cl and DM-Re at 300 K, the ratios V/W=1.8 and 2.4, respectively, are consistent with the presence of a weak Drude component. In the insulat-

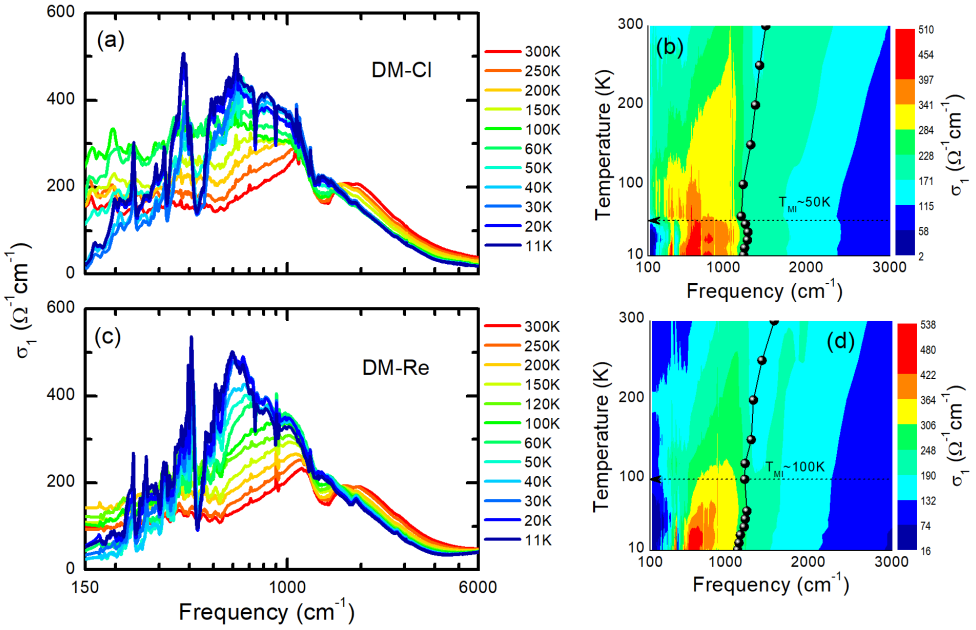

Figure 3. Temperature dependence of the in-plane optical conductivity $\sigma_1(\omega)$ in DM-Cl (a, b) and DM-Re (c, d), showing a temperature-dependent redistribution of spectral weight with decreasing temperature. Panels (a) and (c) display the optical conductivity spectra over a broad frequency range. Panels (b) and (d) present contour plots of $\sigma_1(\omega, T)$, with color maps representing conductivity values up to 3000 cm^{-1}. A suppression of low-frequency conductivity below the metal–insulator transition temperature T_{MI}, indicated by dashed horizontal lines and arrows, reflects the opening of an optical gap around 150 cm^{-1} for DM-Cl and 250 cm^{-1} for DM-Re. Black circles trace the center of spectral weight $<\omega>$, calculated below 3000 cm^{-1}, with the connecting line serving as a guide to its evolution. A logarithmic frequency scale is used in panels (a) and (c) to emphasize low-frequency features.

Table I. Coulomb repulsion V and bandwidth W (in meV and cm^{-1}) along with their ratio V/W, estimated for the Mott–Hubbard band in DM-Cl and DM-Re at 300 K (metallic phase) and 11 K (insulating phase). Values in parentheses are given in cm^{-1}.

Compound, temperature	V	W	V/W
DM-Cl, 300 K (metal)	160 (1290)	88 (710)	1.8
DM-Cl, 11 K (insulator)	73 (590)	20 (160)	3.7
DM-Re, 300 K (metal)	177 (1430)	75 (605)	2.4
DM-Re, 11 K (insulator)	73 (590)	20 (160)	3.7

ing phase at 11 K, both V and W decrease, leading to an increased correlation strength of $V/W = 3.7$ for both materials. The remarkably narrow bandwidth at 11 K results from the increase of the effective carrier mass, reflecting enhanced electronic correlations. This behavior aligns with the onset of charge ordering. Notably, the low-temperature spectra of DM-Cl and DM-Re closely resemble the optical response observed in certain β''-type BEDT-TTF salts in the charge-ordered insulating phase [26, 30].

B. DM-EDT-TTF vibrations in Raman spectra: Charge-order

Vibrational spectroscopy is widely regarded as a prime technique for investigating charge-ordered states in low-dimensional organic conductors [31–36]. This approach is sufficiently sensitive to differentiate between static charge ordering and charge fluctuations [35]. In particular, the extensively studied BEDT-TTF-based materials, feature two charge-sensitive C=C stretching modes in the 1400–1600 cm^{-1} frequency range that are commonly used for this purpose: the ν_2 (a_g) mode, accessible through Raman spectroscopy, and the ν_{27} (b_{1u}) mode, observed in infrared spectra. The ν_{27} mode is especially reliable as a charge-sensitive indicator, although it is typically measurable only in the out-of-plane configuration. However, in certain BEDT-TTF salts, ν_{27} can also be Raman-active, allowing it to serve as an effective probe for charge estimation [36, 37].

The chiral and asymmetric DM-EDT-TTF molecule shares the same tetrathiafulvalene core as the BEDT-TTF and TMTTF donor molecules, suggesting the presence of comparable charge-sensitive modes. Indeed, the C=C stretching modes of DM-EDT-TTF (Fig. 1(b)) have been previously studied and found useful for charge estimation [11, 17]. Consistent with findings for BEDT-

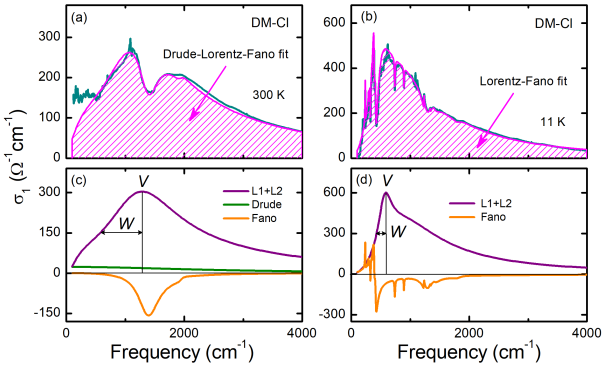

Figure 4. Optical conductivity spectra of DM-Cl fitted using a Drude-Lorentz-Fano model, which includes a Drude term for coherent carriers in the metallic phase (300 K), two Lorentzian components (L1 and L2) representing the mid-infrared Mott-Hubbard band, and multiple Fano terms accounting for intramolecular vibrational modes coupled to the electronic background. Upper panels (a, b) show the experimental data (solid line) and the total fit (shaded area) at 300 K and 11 K, respectively. Lower panels (c, d) display the decomposition of the fit into Drude, Lorentz (L1+L2), and Fano contributions for the same temperatures. The key parameters of the Lorentzian term, the Coulomb repulsion V and the bandwidth W, are marked in panels (c) and (d) as the peak frequency and the low-frequency half-width, respectively [28].

TTF [32, 33, 35, 36], and TMTTF [31, 34], we assume a linear frequency dependence on charge for ν_2 and ν_{27} [11, 32] (inset in Fig. S3(a) in Supplementary Information [29]). However, this does not hold for symmetric ν_3, which strongly interacts with ν_2 within the structure due to coupling with electronic background [32, 35].

In this study, we employ Raman spectroscopy to detect charge-ordered states in DM-Cl and DM-Re. Figure 5 presents the temperature evolution of the Raman spectra of DM-Cl, recorded in two separate experiments using excitation wavelengths of $\lambda = 633$ nm (Fig. 5(a)) and 785 nm (Fig. 5(b)), within the frequency range corresponding to the C=C stretching modes of DM-EDT-TTF [38]. At 200 K, the spectra reveal two distinct features, similar to those observed in various BEDT-TTF salts [2], and in the molecular conductor (*rac*-DM-EDT-TTF)$_2$PF$_6$, which also incorporates the chiral DM-EDT-TTF but in racemic structure [17]. Based on previous experimental findings [11, 17], density functional theory (DFT) calculations [11], and established BEDT-TTF assignments [32, 35], we attribute the asymmetric band at 1485 cm^{-1} to combined ν_3 and ν_{27}, and the band at 1518 cm^{-1} to the ν_2 mode of DM-EDT-TTF with a charge of $+0.5e$.

As the temperature decreases to about 30 K, these features gradually narrow, exhibit pronounced splitting, indicative of charge ordering, and continue to sharpen with further cooling. On the onset of splitting, three ν_2 components are present between 1510 and 1530 cm^{-1}. With further temperature lowering, two satellite peaks ν_2^{max} and ν_2^{min} of $\nu_2^{+0.5}$ gradually grow at the expense of the middle component characteristic for the metallic phase (Fig. S3(d) in Supplementary Information [29]). Here, ν_2^{max} is related with charge-poor DM-EDT-TTF$^{+0.5-\delta}$ molecule, and ν_2^{min} with charge-rich DM-EDT-TTF$^{+0.5+\delta}$ molecule. At 10 K we identify two components of ν_2, along with two components of the ν_{27} mode related with charges $+0.5$-δ and $+0.5$+δ, ν_{27}^{max} and ν_{27}^{min} respectively. The temperature dependence of the ν_2 and ν_{27} mode frequencies is illustrated in Fig. 5(c), that shows a similar splitting for ν_2 and ν_{27}, with increasing frequency separation on the temperature decrease in the insulating phase.

Two discrepancies merit discussion. First, there is a difference in T_{MI}: in the optical experiment, the insulating response emerges below 50 K (Fig. 3(b)), whereas in the Raman study, the first signs of splitting appear below 40 K [39]. The second issue concerns a wavelength-dependent dispersion in Raman band positions observed for ν_2 frequencies (Fig. 5(c)). Such an effect is common in molecular conductors due to vibrational modes interacting with the electronic background. For quantitative analysis, we focus on the experiment with 633 nm excitation, as it provides more reliable data due to lower noise level and the availability of reference data [11].

Charge disproportionation 2δ between the charge-rich DM-EDT-TTF$^{+0.5+\delta}$ and charge-poor DM-EDT-TTF$^{+0.5-\delta}$ can be determined from the frequency splitting [11, 29]. Figure 5(d) presents the charge separation 2δ calculated from the data in Fig. 5(c), as a function of temperature. Notably, in the insulating phase, 2δ increases slightly as the temperature decreases, reaching its maximum at the lowest temperature. This effect can be attributed to enhanced electron correlations, reflected in the increasing effective V/W ratio. From the $\lambda = 633$ nm experiment at 10 K, $2\delta = 0.10e$ based on the ν_2 splitting of 8 cm^{-1} and $2\delta = 0.11e$ from the ν_{27} splitting of 13.7 cm^{-1}. In contrast, charge separation at 10 K, estimated from the ν_2 splitting of 11.4 cm^{-1} in the $\lambda = 785$ nm experiment, gives a slightly higher value of $0.14e$ [40]. However, the overall temperature dependence confirms the results obtained with $\lambda = 633$ nm.

Given the accuracy of our estimates [40], and considering that the lower-frequency component ν_{27}^{min} may be influenced by coupling with the nearby ν_3, we conclude that the charge disproportionation in DM-Cl at 10 K is $0.10e$. The slightly larger splitting of the ν_2 mode observed in DM-Re yields an estimated $2\delta = 0.13e$ (Fig. S3 in Supplementary Information [29]). Interestingly, while charge ordering in DM-Re is consistent with predictions from the low-temperature band structure calculations, its presence in DM-Cl is less expected [16]. We suggest that CO in DM-Cl may arise from subtle inter-site Coulomb interactions (V) within the conducting plane, which are not always fully captured by band-structure methods. In addition, nearly uniform molecular stacks in quarter-filled organic conductors — as found in both

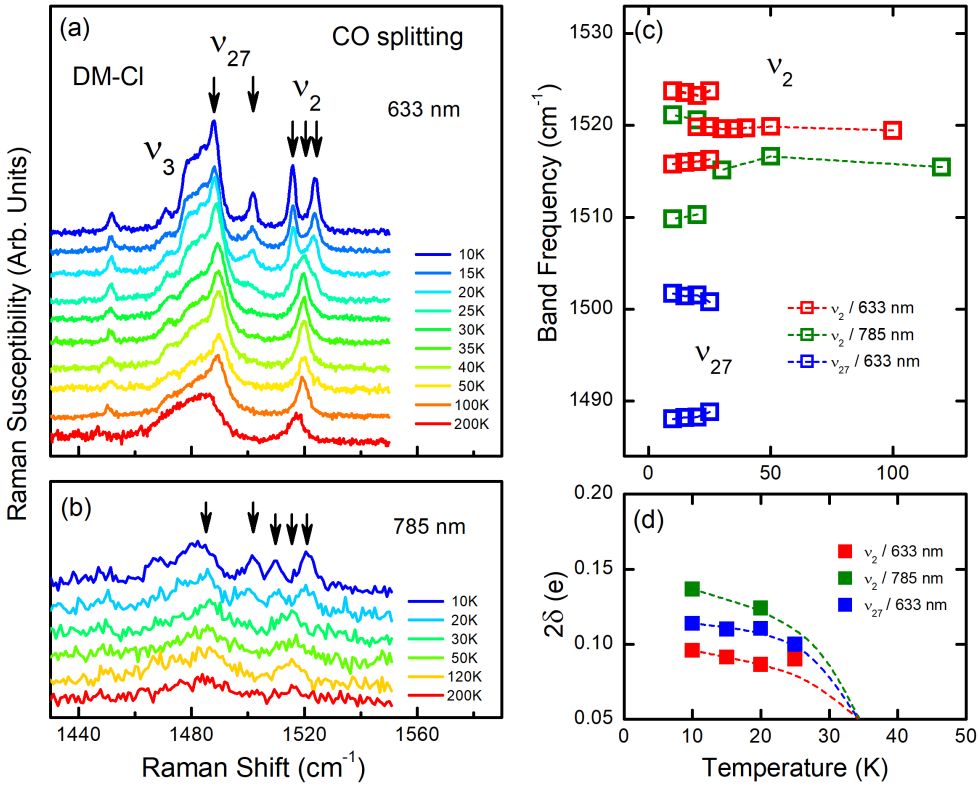

Figure 5. Charge ordering in DM-Cl as revealed by the splitting of charge-sensitive C=C stretching modes ν_2 and ν_{27} of DM-EDT-TTF, measured with excitation wavelengths $\lambda = 633$ nm (a) and 785 nm (b); spectra are vertically offset for clarity. (c) Temperature dependence of the ν_2 and ν_{27} mode frequencies determined by Lorentzian fits to the data in panels (a) and (b). In the ν_2 region (1510-1530 cm^{-1}), two satellite bands emerge at low temperatures alongside the central band associated with the DM-EDT-TTF$^{+0.5}$ species. The high frequency component ν_2^{max} is assigned to charge-poor DM-EDT-TTF$^{+0.5-\delta}$, and the low-frequency component ν_2^{min} to charge-rich DM-EDT-TTF$^{+0.5+\delta}$. For ν_{27} (1485-1505 cm^{-1}), only the low-temperature split components ν_{27}^{max} and ν_{27}^{min} are observed, corresponding to the same charge states. (d) Temperature dependence of the molecular charge separation 2δ, derived from the frequency differences $\nu_2^{max} - \nu_2^{min}$ and $\nu_{27}^{max} - \nu_{27}^{min}$. The charge separation increases slightly with decreasing temperature, reaching $2\delta = 0.10e$ at 10 K based on the ν_2 splitting in the 633 nm data. Dashed lines are guides for the eye.

compounds — are known to be susceptible to CO, as previously observed in model systems such as the θ- and α-type BEDT-TTF salts [41]. Finally, since DM-Cl and DM-Re are isostructural, the presence of CO in one system naturally suggests the possibility of similar behavior in the other. Nonetheless, the relatively small values of charge disproportionation observed in both compounds are comparable to those reported in certain BEDT-TTF salts [26, 37].

C. DM-EDT-TTF vibrations in optical spectra: Electron-molecular vibration coupling

Molecular conductors based on tetrathiafulvalene derivatives, such as BEDT-TTF and TMTTF, are well known for exhibiting strong coupling between totally symmetric molecular vibrations and the electronic background [2, 42]. This electron-molecular vibration (*emv*) coupling modulates the highest occupied molecular orbital (HOMO), often within a dimer unit, gives rise to intense, relatively broad bands in the optical conductivity spectra. These bands appear at significantly shifted frequencies compared to their unperturbed Raman counterparts, enabling estimation of *emv* coupling constants that quantify the interaction strength [36, 42–44]. Because these *emv*-activated features are sensitive to changes in both the electronic state and crystal structure, they serve as effective probes for characterizing phase transitions.

Figure 6(a) presents Raman spectra at 10 K for DM-Cl and DM-Re, in the frequency range of the C-S stretching mode ν_{CS}, often referred to as the C-S "breathing" mode of the DM-EDT-TTF donor molecule [45]. In both compounds, this mode appears as a sharp Raman peak near 500 cm^{-1}. The temperature-dependent optical conductivity spectra of DM-Cl (Fig. 6(b)) and DM-Re (Fig. 6(c)) reveal a broad feature strongly redshifted relative to the unperturbed Raman position. This shift suggests activation of the ν_{CS} mode in the insulating state via electron–molecular vibration (*emv*) coupling. A

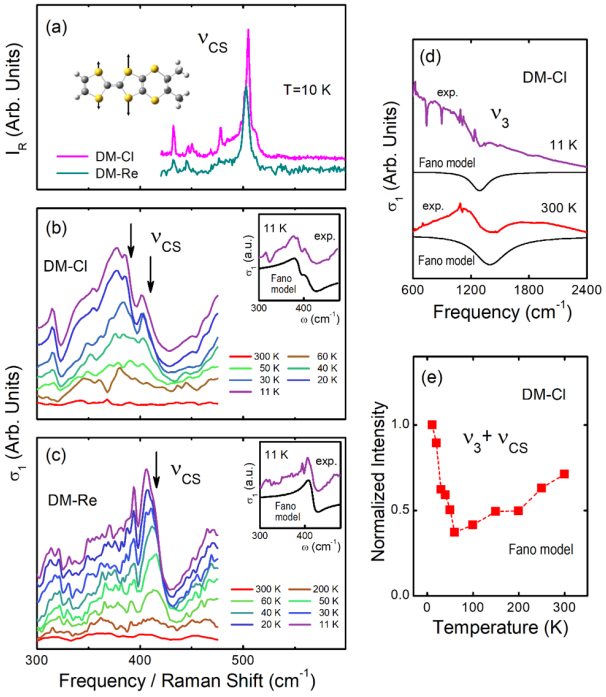

Figure 6. (a) Raman spectra at 10 K for DM-Cl and DM-Re in the frequency range of the C-S "breathing" mode (ν_{CS}) of the DM-EDT-TTF donor molecule. The vibrational mode pattern is shown in the inset. The ν_{CS} mode appears as a sharp peak near 500 cm^{-1} in both compounds. (b, c) Temperature evolution of the optical conductivity spectra for DM-Cl (b) and DM-Re (c), highlighting the activation and redshift of the ν_{CS} mode below the metal–insulator transition temperature T_{MI}, due to electron-molecular vibration (*emv*) coupling with the electronic background. Insets show Fano fits at 11 K: two components were required for DM-Cl (391 and 411 cm^{-1}), while a single component sufficed for DM-Re (416 cm). (d) Optical conductivity spectra of DM-Cl in the mid-infrared region at 11 K and 300 K, showing the ν_3 mode (∼1350 cm^{-1}), also activated via *emv* coupling. Fano fits (black lines) are shown beneath the experimental curves. (e) Temperature dependence of the normalized combined intensity of the ν_3+ν_{CS} modes in DM-Cl, extracted from Fano fits. A strong correlation is observed with the metal–insulator transition at T_{MI} = 50 K. Dashed lines are guides to the eye.

similar *emv*-activated mode has been observed in several BEDT-TTF-based compounds and is commonly labeled as ν_9/ν_{10} [30, 42, 46, 47]. Another *emv*-activated band, observed across the entire temperature range in both materials, is the ν_3 mode near 1350 cm^{-1} (Fig. 6(d)) known for its strong coupling constant [33]. This mode, originally assigned for BEDT-TTF, is shown with its vibrational pattern in Fig. 1(b).

The frequencies of both ν_{CS} and ν_3 mode components in the optical conductivity spectra were estimated using Fano fits within the Drude-Lorentz-Fano model (Chapter IV.A). In the phenomenological Fano model [48], the optical conductivity is expressed with the formula

$$\sigma_1^{Fano}(\nu) = \sigma_0 \frac{\gamma\nu[\gamma\nu(q^2-1)+2q(\nu^2-\nu_0^2)]}{(\nu^2-\nu_0^2)^2+\gamma^2\nu^2}, \quad (1)$$

with the phenomenological coupling parameter q, linewidth γ, the resonance frequency $\nu_0 = \omega_0/2\pi c$, and the spectral weight that describes intensity equal $\int|\sigma_1(\nu)|d\nu$. The significantly broader ν_{CS} mode observed in DM-Cl requires two Fano components for accurate modeling (Fig. 6(b), inset), yielding frequencies of 391 and 411 cm^{-1} at 11 K. In contrast, the narrower ν_{CS} mode in DM-Re is well described by a single Fano component (Fig. 6(c), inset), with a corresponding frequency of 416 cm^{-1} [49]. The substantial redshift of the ν_{CS} mode from its unperturbed Raman position (Fig. 6(a)) - approximately 100 cm^{-1} for DM-Cl and 80 cm^{-1} for DM-Re - along with its pronounced intensity below T_{MI}, suggests a large coupling constant, consistent with values estimated for other TTF-based donor molecules [42].

It is well established that the number of electron–molecular vibration (*emv*)-activated bands associated with a given vibrational mode depends not only on the presence of charge order, as observed in both DM-Cl and DM-Re, but also on subtle structural features that reflect the underlying intermolecular interactions within the conducting layer [50]. While DM-Cl and DM-Re are isostructural and exhibit similar charge disproportionation amplitudes (0.10e vs 0.13e), only DM-Cl shows a clearly resolved doublet in the ν_{CS} mode. In principle, this splitting should appear in both compounds if driven solely by charge disproportionation. However, the observed spectral features also depend on the strength of electron–molecular vibration (*emv*) coupling and on experimental limitations such as the approximations of the fitting model. A weaker splitting in DM-Re cannot be ruled out. We suggest that the key difference lies in the strength of *emv* coupling: in DM-Re, the ν_{CS} mode appears at 416 cm^{-1} at 11 K, much closer to its unperturbed Raman position (∼500 cm^{-1}), while in DM-Cl it forms a pronounced doublet at 391/411 cm^{-1}. This larger redshift in DM-Cl indicates stronger *emv* coupling. We further note that X-ray diffraction measurements (Ref. [16]) reveal significantly higher structural disorder in DM-Re compared to DM-Cl. Such disorder may suppress coherent charge-lattice coupling and could account for the reduced *emv* coupling strength and the absence of clearly resolved mode splitting in DM-Re.

Notably, the temperature evolution of the frequency separation between the two ν_{CS} components in DM-Cl (Fig. S4(c) in Supplementary Information [29]) closely resembles that of the charge-sensitive ν_2 and ν_{27} Raman modes (Fig. 5(c)). While the ν_{CS} mode in optical spectra is primarily influenced by structural factors, it is also charge-sensitive, with a calculated frequency shift of 23 cm^{-1} upon ionization from the neutral species to DM-EDT-TTF^{+1}, according to DFT results [45]. We therefore suggest that the observed frequency splitting of the ν_{CS} mode arises from a combination of structural distor-

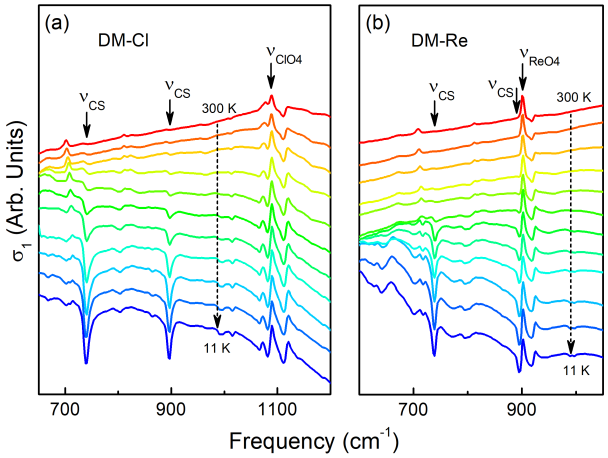

Figure 7. Temperature-dependent optical conductivity spectra of DM-Cl (a) and DM-Re (b) in the frequency range corresponding to vibrational modes of the tetrahedral anions ClO_4 and ReO_4, respectively. In panel (a), ClO_4 modes appear near 1100 cm^{-1}, while in panel (b), ReO_4 modes are centered around 900 cm^{-1}. At lower frequencies, both compounds exhibit features associated with the C–S stretching modes (ν_{CS}) of the DM-EDT-TTF donor molecule. Spectra are vertically offset for clarity, with temperature decreasing from 300 K (top) to 11 K (bottom).

tions and underlying charge ordering.

Figure 6(d) displays the experimental optical conductivity spectra of DM-Cl in the frequency range of the ν_3 mode at 11 and 300 K, along with corresponding Fano fits using a single Fano component. The coupling parameter q was found to be zero at all temperatures, indicating symmetric coupling. While the antiresonance exhibits higher intensity at elevated temperatures - likely due to overlap with the mid-infrared band - it remains consistently active across the full temperature range in both DM-Cl and DM-Re. This behavior suggests that the strong temperature dependence of *emv*-activated vibrational features is predominantly governed by changes in the electronic background rather than by significant structural modifications. Indeed, the ν_3 antiresonance exhibits a monotonic redshift upon cooling in both compounds (Fig. S4(a) in Supplementary Information [29]). In contrast, the appearance of the ν_{CS} mode is more directly linked to the metal–insulator transition. One contributing factor is the reduction in electronic screening below T_{MI}, while another is the emergence of a mid-infrared band centered near 600 cm^{-1} at low temperatures in both systems. As a result, the temperature dependence of the normalized combined intensity of the ν_3+ν_{CS} modes in DM-Cl, extracted from Fano fits, shows a pronounced anomaly at T_{MI}=50 K (Fig. 6(e)). A separate comparison of the individual ν_3 and ν_{CS} intensities is provided in Fig. S4(b) of the Supplementary Information [29].

While the DM-EDT-TTF vibrational modes in DM-Cl and DM-Re are largely screened in the metallic phase, the characteristic molecular vibrations of the tetrahedral ClO_4 and ReO_4 anions persist in the optical conductivity spectra across the entire temperature range, appearing at 1100 cm^{-1} (ClO_4, Fig. 7(a)) and ∼900 cm^{-1} (ReO_4, Fig. 7(b)). These anion modes exhibit only weak interaction with the electronic background, minimal temperature dependence, and no correlation with the metal-insulator transition. This suggests that, unlike most low-dimensional charge-transfer salts based on TTF-derived donor molecules [51], the anion network plays a negligible role in governing the conducting properties of both DM-Cl and DM-Re.

V. CONCLUSIONS

This study confirms the charge-ordered nature of the insulating state in the chiral molecular conductors DM-Cl and DM-Re, with a charge disproportionation of 0.10e and 0.13e, respectively, as determined from the splitting of charge-sensitive DM-EDT-TTF modes in the Raman spectra of the insulating phase. The optical conductivity spectra reveal the formation of an insulating gap at the metal-insulator transition, with Δ_{MI} = 150 and 250 cm^{-1} for DM-Cl and DM-Re, respectively. From the analysis of our optical spectra we conclude that intersite Coulomb repulsion V is the dominant interaction driving this transition. Additionally, both compounds exhibit strong vibrational DM-EDT-TTF features resulting from coupling with the electronic background, underscoring the complexity of intermolecular interactions in the conducting layer. These findings provide new insights into the role of molecular structure and Coulomb interactions in stabilizing charge ordering in these low-dimensional conductors, paving the way for further studies on related systems.

ACKNOWLEDGMENTS

N. A., I. O. and A. F. thank the Narodowa Agencja Wymiany Akademickiej – NAWA (Poland, BPN/BFR/2021/1/00001/U/00001) and the French Ministry of Foreign Affairs and the French Ministry of Education and Research (France, PHC Project 48119PG) for financial support through the bilateral Polonium project. The work in Poland was supported within the Statutory Activities of the Institute of Molecular Physics Polish Academy of Sciences and partially supported at Poznan University of Technology by the Research Project of the Polish Ministry of Education and Science 0511/SBAD/2251. We acknowledge funding by the Deutsche Forschungsgemeinschaft via Grant No. Dr 228/39-3 and Dr 228/63-1. We acknowledge the technical support from Gabrielle Untereiner and Svenja Wörfel.

[1] J. M. Williams, J. R. Ferraro, R. J. Thorn, K. D. Carlson, U. Geiser, H. H. Wang, A. M. Kini, and M. H. Whangbo, *Organic Superconductors (Including Fullerenes)* (Prentice Hall: Englewood Cliffs, 1992).

[2] M. Dressel and N. Drichko, Optical properties of two-dimensional organic conductors: Signatures of charge ordering and correlation effects, Chem. Rev. **104**, 5689 (2004).

[3] B. J. Powell and R. H. McKenzie, Quantum frustration in organic mott insulators: from spin liquids to unconventional superconductors, Rep. Prog. Phys. **74**, 056501 (2011).

[4] M. Dressel and S. Tomić, Molecular quantum materials: electronic phases and charge dynamics in two-dimensional organic solids, Adv. Phys. **69**, 1 (2020).

[5] A. Pustogow, M. Bories, A. Löhle, R. Rösslhuber, E. Zhukova, B. Gorshunov, S. Tomić, J. A. Schlueter, R. Hübner, T. Hiramatsu, Y. Yoshida, G. Saito, R. Kato, T.-H. Lee, V. Dobrosavljević, S. Fratini, and M. Dressel, Quantum spin liquids unveil the genuine Mott state, Nat. Mater. **17**, 773–777 (2018).

[6] S. Iwai, K. Yamamoto, A. Kashiwazaki, F. Hiramatsu, H. Nakaya, Y. Kawakami, K. Yakushi, H. Okamoto, H. Mori, and Y. Nishio, Photoinduced melting of a stripe-type charge-order and metallic domain formation in a layered BEDT-TTF-based organic salt, Phys. Rev. Lett. **98**, 097402 (2007).

[7] Y. Kawakami, T. Fukatsu, Y. Sakurai, H. Unno, H. Itoh, S. Iwai, T. Sasaki, K. Yamamoto, K. Yakushi, and K. Yonemitsu, Early-stage dynamics of light-matter interaction leading to the insulator-to-metal transition in a charge ordered organic crystal, Phys. Rev. Lett. **105**, 246402 (2010).

[8] M. Buzzi, D. Nicoletti, M. Fechner, N. Tancogne-Dejean, M. A. Sentef, A. Georges, T. Biesner, E. Uykur, M. Dressel, A. Henderson, T. Siegrist, J. A. Schlueter, K. Miyagawa, K. Kanoda, M.-S. Nam, A. Ardavan, J. Coulthard, J. Tindall, F. Schlawin, D. Jaksch, and A. Cavalleri, Photomolecular high-temperature superconductivity, Phys. Rev. X **10**, 031028 (2020).

[9] F. Pop, N. Zigon, and N. Avarvari, Main-group-based electro- and photoactive chiral materials, Chem. Rev. **119**, 8435 (2019).

[10] F. Pop, P. Auban-Senzier, E. Canadell, G. L. J. A. Rikken, and N. Avarvari, Electrical magnetochiral anisotropy in a bulk chiral molecular conductor, Nat. Commun. **5**, 3757 (2014).

[11] F. Pop, P. Auban-Senzier, A. Frąckowiak, K. Ptaszyński, I. Olejniczak, J. D. Wallis, E. Canadell, and N. Avarvari, Chirality driven metallic versus semiconducting behavior in a complete series of radical cation salts based on dimethyl-ethylenedithio-tetrathiafulvalene (DM-EDT-TTF), J. Am. Chem. Soc. **135**, 17176 (2013).

[12] F. Pop, P. Auban-Senzier, E. Canadell, and N. Avarvari, Anion size control of the packing in the metallic versus semiconducting chiral radical cation salts (DM-EDT-TTF)$_2$XF$_6$ (X = P, As, Sb), Chem. Commun. **52**, 12438 (2016).

[13] N. Mroweh, C. Mézière, F. Pop, P. Auban-Senzier, P. Alemany, E. Canadell, and N. Avarvari, In search of chiral molecular superconductors: κ-[(S,S)-DM-BEDT-TTF]$_2$ClO$_4$ revisited, Adv. Mater. **32**, 2002811 (2020).

[14] D. Branzea, F. Pop, P. Auban-Senzier, R. Clérac, P. Alemany, E. Canadell, and N. Avarvari, Localization versus delocalization in chiral single component conductors of gold bis(dithiolene) complexes, J. Am. Chem. Soc. **138**, 6838 (2016).

[15] F. Pop and N. Avarvari, Chiral metal-dithiolene complexes, Coordin. Chem. Rev. **346**, 20 (2017).

[16] F. Pop, N. Mroweh, P. Auban-Senzier, G. L. J. A. Rikken, D. Hirobe, H. M. Yamamoto, A. Frąckowiak, I. Olejniczak, S. Pillet, E.-E. Bendeif, P. Alemany, E. Canadell, and N. Avarvari, Chiral metallic DM-EDT-TTF radical cation salts: Anion size dependent structural and electronic transitions, charge ordering and chirality induced spin selectivity, J. Am. Chem. Soc. submitted.

[17] I. Olejniczak, A. Frąckowiak, K. Ptaszyński, F. Pop, and N. Avarvari, Charge fluctuations in the dimer-mott insulating state of (*rac*-DM-EDT-TTF)$_2$PF$_6$, J. Phys. Chem. C **121**, 21975 (2017).

[18] M. Dressel and G. Grüner, *Electrodynamics of Solids: Optical Properties of Electrons in Matter* (Cambridge University Press, 2002).

[19] D. Faltermeier, J. Barz, M. Dumm, M. Dressel, N. Drichko, B. Petrov, V. Semkin, R. Vlasova, C. Meźière, and P. Batail, Bandwidth-controlled Mott transition in κ-(BEDT-TTF)$_2$Cu[N(CN)$_2$]Br$_x$Cl$_{1-x}$: Optical studies of localized charge excitations, Phys. Rev. B **76**, 165113 (2007).

[20] M. J. Rice, N. O. Lipari, and S. Strässler, Dimerized organic linear-chain conductors and the unambiguous experimental determination of electron-molecular-vibration coupling constants, Phys. Rev. Lett. **39**, 1359 (1977).

[21] Due to the lack of data below 120 cm^{-1} and insuficcient sensitivity of reflectivity experiment below 300 cm^{-1}, zero-frequency optical conductivity values at 300 K are larger than expected 10-30 Ω^{-1}cm^{-1} both for DM-Cl and DM-Re.[16].

[22] A. Georges, G. Kotliar, W. Krauth, and M. J. Rozenberg, Dynamical mean-field theory of strongly correlated fermion systems and the limit of infinite dimensions, Rev. Mod. Phys. **68**, 13 (1996).

[23] M. J. Rozenberg, G. Kotliar, and H. Kajueter, Transfer of spectral weight in spectroscopies of correlated electron systems, Phys. Rev. B **54**, 8452 (1996).

[24] H. Benthien and E. Jeckelmann, Optical conductivity of the one-dimensional dimerized Hubbard model at quarter filling, Eur. Phys. J. B **44**, 287 (2005).

[25] A. Pustogow, *Unveiling Electronic Correlations in Layered Molecular Conductors by Optical Spectroscopy*, Ph.D. thesis, University of Stuttgart (2017).

[26] A. Pustogow, K. Treptow, Y. Rohwer, A. Saito, M. Sanz Alonso, A. Löhle, J. A. Schlueter, and M. Dressel, Charge order in β''-phase BEDT-TTF salts, Phys. Rev. B **99**, 155144 (2019).

[27] While elementary excitations involving double occupancy within the charge-ordered pattern are described by the Mott-Hubbard band centered at an energy of U-V, other excitations are associated with the band centered at V. Both U-V and V depend on the specific molecular interactions within the conducting layer and should be considered as effective values.

[28] In quarter-filled salts, the Mott-Hubbard band tends to be asymmetric due to uneven charge occupancy, while its high-frequency tail is influenced by additional contributions. Therefore, to estimate the bandwidth W of this band in DM-Cl and DM-Re, we use the low-frequency part of the Lorentzian component.

[29] See the Supplementary Information at [URL] for figures presenting optical and Raman spectra other than shown in the main text, as well as some additional discussion.

[30] W. Li, E. Rose, M. V. Tran, R. Hübner, A. Łapiński, R. Świetlik, S. A. Torunova, E. I. Zhilyaeva, R. N. Lyubovskaya, and M. Dressel, The metal-insulator transition in the organic conductor β''-(BEDT-TTF)$_2$Hg(SCN)$_2$Cl, J. Chem. Phys. **147**, 064503 (2017).

[31] M. Meneghetti, R. Bozio, I. Zanon, C. Pecile, C. Ricotta, and M. Zanetti, Vibrational behavior of molecular constituents of organic superconductors: TMTSF, its radical cation and the sulphur analogs TMTTF and TMTTF$^+$, J. Chem. Phys. **80**, 6210 (1984).

[32] T. Yamamoto, M. Uruichi, K. Yamamoto, K. Yakushi, A. Kawamoto, and H. Taniguchi, Examination of the charge-sensitive vibrational modes in bis(ethylenedithio)tetrathiafulvalene, J. Phys. Chem. B **109**, 15226 (2005).

[33] A. Girlando, Charge sensitive vibrations and electron-molecular vibrational coupling in bis(ethylenedithio)-tetrathiafulvalene (BEDT-TTF), J. Phys. Chem. C **115**, 19371 (2011).

[34] M. Dressel, M. Dumm, T. Knoblauch, and M. Masino, Comprehensive optical investigations of charge order in organic chain compounds (TMTTF)$_2$X, Crystals **2**, 528 (2012).

[35] A. Girlando, M. Masino, J. A. Schlueter, N. Drichko, S. Kaiser, and M. Dressel, Examination of the charge-sensitive vibrational modes in bis(ethylenedithio)tetrathiafulvalene, Phys. Rev. B **89**, 174503 (2014).

[36] A. Girlando, Raman signatures of the strong intramolecular and intermolecular charge oscillations in bis(ethylenedithio)-tetrathiafulvalene (BEDT-TTF)κ-phase salts, Phys. Rev. B **110**, 035101 (2024).

[37] I. Olejniczak, R. Wesołowski, H. O. Jeschke, R. Valentí, B. Barszcz, and J. A. Schlueter, Charge ordering and low-temperature lattice distortion in the β'-(BEDT-TTF)$_2$CF$_3$CF$_2$SO$_3$ dimer Mott insulator, Phys. Rev. B **101**, 035150 (2020).

[38] Portions of the Raman data presented here (spectra measured with $\lambda = 633$ nm excitation) will also be included, in part, in a complementary study on structural and electronic aspects of chiral molecular conductors, currently in preparation for submission to JACS (Ref. [16]).

[39] Two factors affect temperature readings in the Raman experiment. The first is sample heating, which occurs even at very low laser power due to the submillimeter sample size. The second issue arises from the placement of the temperature sensor on a cold finger, positioned farther from the sample, whereas in the optical setup, it is much closer. As a result, temperature readings in the Raman experiment are less reliable.

[40] To calculate the charge separation 2δ for Raman data measured with a $\lambda = 785$ nm excitation wavelenght, we use Eq. (1) based on the splitting between the neutral DM-EDT-TTF and DM-EDT-TTF^{+1} measured with $\lambda = 633$ nm. This approach introduces an error that is difficult to quantify. Consequently, the 2δ value estimated from the 785 nm data is less reliable.

[41] K. Yakushi, Infrared and Raman studies of charge ordering in organic conductors, BEDT-TTF salts with quarter-filled bands, Crystals **2**, 1291 (2012).

[42] G. Visentini, M. Masino, C. Bellitto, and A. Girlando, Experimental determination of BEDT-TTF$^+$ electron-molecular vibration constants through optical microreflectance, Phys. Rev. B **58**, 9460 (1998).

[43] M. Rice, Towards the experimental determination of the fundamental microscopic parameters of organic ion-radical compounds, Solid State Commun. **31**, 93 (1979).

[44] A. Painelli and A. Girlando, Electron–molecular vibration (e–mv) coupling in charge-transfer compounds and its consequences on the optical spectra: A theoretical framework, J. Chem. Phys. **84**, 5655 (1986).

[45] A. Frąckowiak, I. Olejniczak, N. Avarvari, unpublished results.

[46] N. Drichko, M. Dressel, C. A. Kuntscher, A. Pashkin, A. Greco, J. Merino, and J. Schlueter, Electronic properties of correlated metals in the vicinity of a charge-order transition: Optical spectroscopy of α-(BEDT-TTF)$_2$MHg(SCN)$_4$ (M = NH$_4$, Rb, Tl), Phys. Rev. B **74**, 235121 (2006).

[47] T. Ivek, B. Korin-Hamzić, O. Milat, S. Tomić, C. Clauss, N. Drichko, D. Schweitzer, and M. Dressel, Electrodynamic response of the charge ordering phase: Dielectric and optical studies of α-(BEDT-TTF)$_2$I$_3$, Phys. Rev. B **83**, 165128 (2011).

[48] U. Fano, Effects of configuration interaction on intensities and phase shifts, Phys. Rev. **124**, 1866 (1961).

[49] During fitting with the Drude-Lorentz-Fano model, both DM-Cl and DM-Re were tested for one and two ν_{CS} components. Within the margin of error, the analysis revealed that two components are necessary for DM-Cl, while only one is sufficient for DM-Re.

[50] M. Meneghetti, C. Pecile, K. Yakushi, K. Yamamoto, K. Kanoda, and K. Hiraki, Study of the phase transitions of (DI-DCNQI)$_2$M (M=Ag, Li, Cu) through the analysis of the temperature-dependent vibronic and vibrational infrared absorptions, J. Solid State Chem. **168**, 632 (2002).

[51] J.-P. Pouget, Interplay between electronic and structural degrees of freedom in quarter-filled low dimensional conductors, Physica B **460**, 45 (2015).